AGU PUBLICATIONS

JGR

Journal of Geophysical Research: Atmospheres

RESEARCH ARTICLE
10.1002/2013JD020307

Key Points:
- Improvement of the ^{222}Rn tracer inversion method
- CO_2 emissions in Bern are estimated at: 11.2 kt km^{-2} a^{-1}
- Hourly CO_2 flux and OR show temporal and spatial variability of sources

Supporting Information:
- Readme
- Supporting information on selected event: Tables S1–S3 and Figures S1–S3

Correspondence to:
S. van der Laan,
svanderlaan@climate.unibe.ch;
svanderlaan1978@gmail.com

Citation:
van der Laan, S., I. T. van der Laan-Luijkx, L. Zimmermann, F. Conen, and M. Leuenberger (2014), Net CO_2 surface emissions at Bern, Switzerland inferred from ambient observations of CO_2, $\delta(O_2/N_2)$, and ^{222}Rn using a customized radon tracer inversion, *J. Geophys. Res. Atmos.*, *119*, 1580–1591, doi:10.1002/2013JD020307.

Received 3 JUN 2013
Accepted 8 JAN 2014
Accepted article online 14 JAN 2014
Published online 5 FEB 2014

Net CO_2 surface emissions at Bern, Switzerland inferred from ambient observations of CO_2, $\delta(O_2/N_2)$, and ^{222}Rn using a customized radon tracer inversion

S. van der Laan[1], I. T. van der Laan-Luijkx[1,2], L. Zimmermann[3], F. Conen[3], and M. Leuenberger[1]

[1]Physics Institute and Oeschger Centre for Climate Change Research, University of Bern, Bern, Switzerland, [2]Now at Meteorology and Air Quality, Wageningen University, Wageningen, Netherlands, [3]Department of Environmental Sciences, University of Basel, Basel, Switzerland

Abstract The ^{222}Radon tracer method is a powerful tool to estimate local and regional surface emissions of, e.g., greenhouse gases. In this paper we demonstrate that in practice, the method as it is commonly used, produces inaccurate results in case of nonhomogeneously spread emission sources, and we propose a different approach to account for this. We have applied the new methodology to ambient observations of CO_2 and ^{222}Radon to estimate CO_2 surface emissions for the city of Bern, Switzerland. Furthermore, by utilizing combined measurements of CO_2 and $\delta(O_2/N_2)$ we obtain valuable information about the spatial and temporal variability of the main emission sources. Mean net CO_2 emissions based on 2 years of observations are estimated at (11.2 ± 2.9) kt km^{-2} a^{-1}. Oxidative ratios indicate a significant influence from the regional biosphere in summer/spring and fossil fuel combustion processes in winter/autumn. Our data indicate that the emissions from fossil fuels are, to a large degree, related to the combustion of natural gas which is used for heating purposes.

1. Introduction

The ^{222}Radon (^{222}Rn) tracer method is a powerful tool to determine local-regional surface fluxes because it can be applied to a wide range of (e.g., greenhouse) gases, and most importantly, because it is a purely observationally based approach. The method revolves around ^{222}Rn, a radioactive noble gas that is produced at a constant rate from ^{226}Radium, which is relatively uniformly distributed in all soils. When released into the atmosphere, ^{222}Rn experiences the same atmospheric circumstances (transport and mixing) as all other gases. If the ^{222}Rn surface flux is known, its ratio to a measured ^{222}Rn concentration difference over time at a certain observation height can be applied to calculate the surface flux of another constituent (e.g., CO_2) from its concurrently observed concentration difference at the same height. The method has been successfully applied for a wide range of gases such as CO_2 [*Levin*, 1987; *Schmidt et al.*, 2001], CH_4 [*Schmidt et al.*, 1996; *van der Laan et al.*, 2009], N_2O [*van der Laan et al.*, 2009; *Wilson et al.*, 1997], CFCs [*Biraud et al.*, 2000], H_2 [*Popa et al.*, 2011; *Yver et al.*, 2010], and fossil fuel-based CO_2 [*van der Laan et al.*, 2010]. Generally, a constant ^{222}Rn soil emission rate is assumed and multiplied by the ratio of observed CO_2 and ^{222}Rn concentrations. This ratio is usually determined with a linear regression fit of the observations within specific periods: e.g., monthly means [*Levin*, 1987], nighttime-restricted data [*Schmidt et al.*, 2001; *Yver et al.*, 2010], or specific events of sudden concentration enhancements [*Biraud et al.*, 2000]. The latter approach has the advantage that it allows for source allocation by back trajectory analysis [*Messager et al.*, 2008; *van der Laan et al.*, 2009]. The resulting CO_2 flux is a net flux integrated over the observed source region (footprint) and the observation time and weighted toward the sensitivity of the observations to the emission sources [*Hirsch*, 2007].

In section 2 we will demonstrate that, in practice, the regression slope method does not produce reliable results because it assumes a linear correlation between the ^{222}Rn flux and the flux of the tracer of interest. In practice, this condition is almost never met (e.g., for CO_2) because the emission sources are generally not constant in time and not homogeneously spread within the observed footprint. Therefore, we suggest a customized method (section 2.3) based on using single pair of observations for a given event. This approach was applied to ambient observations of CO_2 and ^{222}Radon to estimate CO_2 surface emissions

for the region of Bern, Switzerland. Furthermore, we use ambient observations of $\delta(O_2/N_2)$ to determine the oxidative ratio (OR) of the CO_2 emissions. The OR identifies the different emission sources (e.g., traffic or natural gas combustion) and sinks (i.e., CO_2 exchange with the biosphere) and provides valuable information regarding the temporal and spatial variability of the main CO_2 sources and sinks in our region. The measurement location and used equipment as well as the data selection procedures are described in section 3, and the results are described in section 4. A discussion and our conclusions follow in section 5.

2. Theory

2.1. ^{222}Rn as a Tool for Atmospheric Inversion Studies

The concept of using ^{222}Rn as a tool to calculate the surface flux of a specie x from their measured ambient concentrations is based on the fact that both species experience the same atmospheric transport and dilution. During well-mixed atmospheric conditions, ambient concentrations are observed at (local) background levels, but during stable conditions the surface fluxes accumulate within the planetary boundary layer leading to a departure from background conditions as follows [*Biraud et al.*, 2000]:

$$\frac{\Delta C_x}{\Delta t} = \int_{t_0}^{t_n} h(t)^{-1}\, \Phi_x(t)\, \mathrm{d}t = \overline{h^{-1}\, \Phi_x} \tag{1}$$

where $h(t)$ is the time dependent mixing height, $\Phi_x(t)$ represents the surface flux of a species x, and ΔC_x is the departure of its related concentration relative to background levels for a given observation time Δt (i.e., $t_n - t_0$). The overbar indicates averaging in space and time, i.e., representing the average mixing height for the observation period and the mean net surface flux of the catchment area. Because equation (1) is obtained both for CO_2 and ^{222}Rn, the mixing height and time step are canceled out yielding

$$\overline{\Phi CO_2} = \frac{\Delta CO_2}{\Delta Rn}\, \overline{\Phi Rn} \tag{2}$$

where ΔCO_2 and ΔRn represent the concentration enhancements of CO_2 and ^{222}Rn from their respective background levels for a given observation period and $\overline{\Phi CO_2}$ and $\overline{\Phi Rn}$ represent the mean surface fluxes of CO_2 and ^{222}Rn of the sources within the observed catchment area. To correct for the decay of ^{222}Rn during its travel to the observation site, the result from equation (2) is multiplied with

$$\frac{1 - e^{-\lambda\, \Delta t}}{\lambda\, \Delta t} \tag{3}$$

where λ is the decay constant of ^{222}Rn (0.182 d^{-1}) and Δt represents the transit time of the air mass from the source to the observation site [*van der Laan et al.*, 2009]. As explained in section 1 it is common procedure to determine the quotient of equation (2) with a linear regression fit on a bulk of CO_2 versus ^{222}Rn observations. In the next section we use a theoretical example to explain why this method yields biased results and in the subsequent section we propose a modified version as a solution to this problem.

2.2. Problem Definition

Consider a theoretical example in which ambient concentrations of CO_2 and ^{222}Rn are sampled at the same height and measured simultaneously (Figure 1a). Starting at local background conditions, both concentrations are observed to rise (Figure 1b) because of increasing atmospheric stability (usually in the late afternoon or at night) accumulating their respective surface emissions in the lower part of the atmosphere. In this simplified example we consider an event consisting of 10 observations of CO_2 and ^{222}Rn concentrations above background levels (i.e., indicated by ΔCO_2 and Δ^{222}Rn, respectively). After the tenth observation, the event ends when atmospheric turbulence is restarted (often observed early in the morning when the Sun rises) and the measured concentrations drop back to their respective

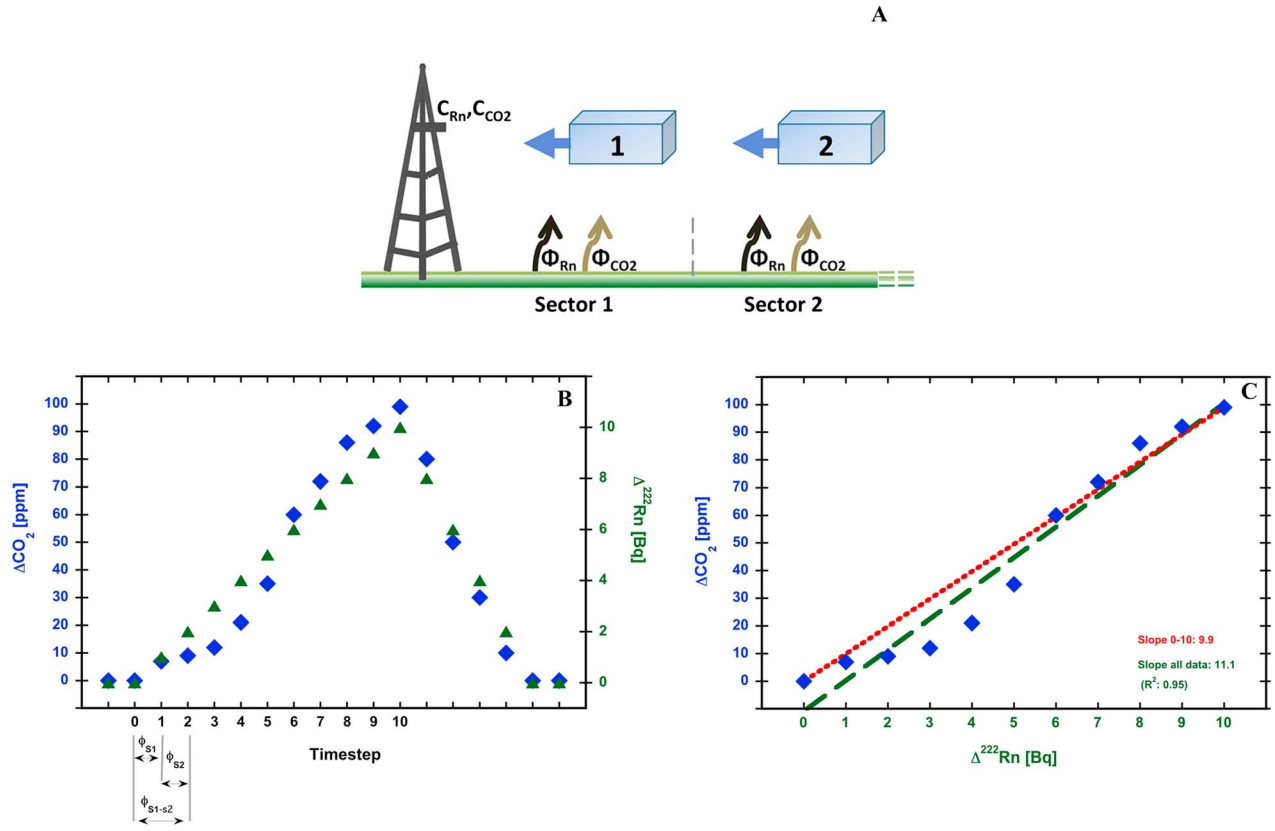

Figure 1. Simplified illustration of (a) CO_2 and ^{222}Rn surface emissions being transported to a measurement tower under stationary conditions, (b) the corresponding observed concentration increases at the site and (c) CO_2 versus ^{222}Rn fitted with a linear regression fit (green dashed line) and comparison with single pair of observations method (red dotted line).

background levels. We further assume a constant wind speed and wind direction during the event such that with each time step t, the surface fluxes of both species (Φ_{CO2} and Φ_{Rn}) are transported from a consecutive distance (defined as sector x_t) to the site. So, with the assumed wind speed the air mass is transported over the area of the size of a sector in each time step. For example, the first concentration increases (at time step 1) represent $\Delta CO_2(t_1)$ and $\Delta Rn(t_1)$ related to Φ_{CO2} and Φ_{Rn} from sector 1. Equally so, Φ_{CO2} and Φ_{Rn} from both sector 1 (for time step 2) and sector 2 (for time step 1, since it takes two time steps for the air to reach the observation site) are collected and integrated by the air mass during its trajectory to the station and observed at time step 2 as $\Delta CO_2(t_2)$ and $\Delta Rn(t_2)$. In Table 1 this example is further illustrated using synthetic surface fluxes for each sector within our catchment area which have been converted to concentration enhancements assuming a mixing height of 50 m. In our example, the mean net CO_2 flux for the total fetch is 8.5 kt km^{-2} a^{-1}. However, using a least squares linear regression fit on all observations (Figure 1c, green dashed line) and applying equation (2) returns a mean flux of 9.6 kt km^{-2} a^{-1}. The mean value given by the regression fit method differs from the arithmetic mean because the CO_2 and ^{222}Rn fluxes are not perfectly correlated. This makes sense because the buildup in concentrations observed in CO_2 and ^{222}Rn are not only related to atmospheric transport and dilution but also to the behavior of their sources which obviously differ. To obtain the arithmetic mean of the prior fluxes using all observations, one should use the average of all individual slopes for each consecutive time step:

$$\overline{\Phi CO_2} = \left(\sum_{n-1}^{n} \frac{CO_2(t_n) - CO_2(t_{n-1})}{Rn(t_n) - Rn(t_{n-1})} \right) \cdot \frac{\overline{\Phi Rn}}{n} \tag{4}$$

which, in Table 1 is demonstrated in the second to the last column. However, such an approach assumes the sources to remain constant in time for the total observation period, a requirement which is rarely fulfilled.

Table 1. Example Illustrating the Difference Between the Commonly Applied Regression Fit Method and the Single Pair of Observations Method With Synthetic Data[a]

	Input Surface Flux		Observed Concentration Difference		Calculated Net Surface Emission (kt km^{-2} a^{-1})		
Time Step (Sector)	Φ_{Rn} (Bq m^{-2} h^{-1})	Φ_{CO2} (kt km^{-2} a^{-1})	ΔRn (Bq)	ΔCO_2 (ppm)	Lin. Regr. ($t_0 \ldots t_{10}$)	Single Pair (t_{n-1}–t_n)	Single Pair t_0–t_n
0			0	0			
1	50	6	1	7		6	6.0
2	50	2	2	9		2	4.0
3	50	2	3	12		2	3.3
4	50	8	4	21		8	4.5
5	50	12	5	35		12	6.0
6	50	22	6	60		22	8.7
7	50	10	7	72		10	8.9
8	50	12	8	86		12	9.3
9	50	5	9	92		5	8.8
10	50	6	10	99		6	8.5
Mean flux total area		8.5			9.6	8.5	8.5

[a]Values are calculated for a mixing height of 50 m using equations (4) and (5) and a conversion factor of 22.4 dm^3 per 1 mol of air.

Note that if the sources would remain stationary, this approach would, theoretically, enable one to calculate sector-specific surface fluxes from their related concentration changes. For example, the slope determined from the observed concentration differences between time steps 1 and 2 represents the mean surface flux for sector 2 specifically.

2.3. Single Pair of Observations Approach

During its transport to the observation site, an air parcel collects and integrates the surface emissions from the underlying sectors and therefore represents the mean surface flux integrated over the total area and the observation time. Therefore, the mean net CO_2 flux for the total catchment area of our example is given by

$$\overline{\Phi CO_2} = \frac{CO_2(t_n) - CO_2(t_0)}{Rn(t_n) - Rn(t_0)} \cdot \overline{\Phi Rn} \tag{5}$$

with t_n corresponding to the observations at the final time step of the event (i.e., 10 in our example) and t_0 representing local background levels. The results for each consecutive observation are given in Table 1 (last column), and the final value is indeed equal to the mean of the prior fluxes (indicated in Figure 1c, red dotted line).

The result from equation (5) represents a net mean flux over the total catchment area and thus relates to the total observation time and the air mass trajectory. For example, if each observation in our example represents an hourly integrated value and the mean wind speed is 2 m s^{-1}, the result represents the mean value for a fetch range of 72 km in distance. This approach to estimate the maximum fetch range assumes the wind speed and direction remain constant during the observation period and can therefore only be applied to local-scale estimates (i.e., short events). For emission estimates involving relatively large distances, back trajectory analysis can be applied to estimate the source regions [e.g., *van der Laan et al.*, 2009]. Note also that the result obtained from equation (5) represents a mean value corresponding to the total observation period but constructed from fluxes emitted at different times. For example, the result from our example represents a mean emission integrated over a period of 10 time steps (i.e., 10 h for hourly integrated observations) but consists of the flux from sector 10 from 10 h ago, the flux from sector 9 from 9 h ago, etc. Therefore, one cannot interpret the results as a single snapshot for the given period but has to take atmospheric transport into account.

In our theoretical example, the difference between the fluxes calculated from our approach and the linear regression fit method is 13% for the whole event. In practice, the difference between the two methods depends highly on the variability and magnitude of the observed emission sources. For example, at our site a mean difference of 32% was found for three randomly chosen events (see supporting information).

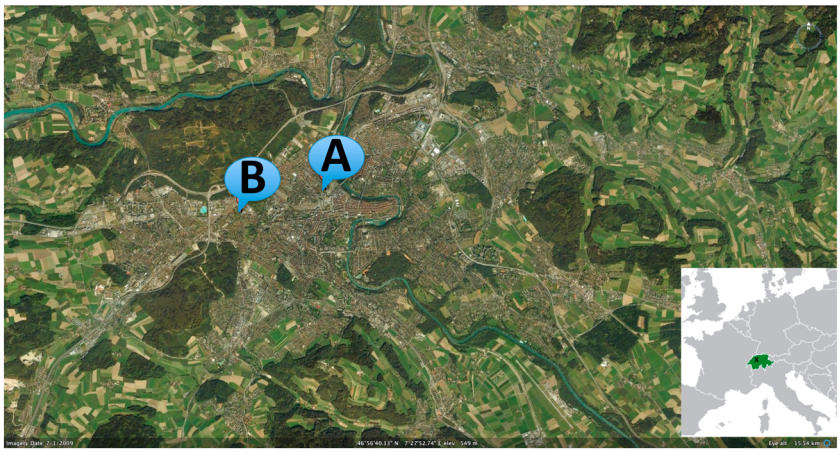

Figure 2. Map of the city of Bern, Switzerland, with (a) our sampling location in the center and (b) a nearby waste incineration facility.

In this study we have estimated surface fluxes for Bern using equation (5). We assumed a constant ^{222}Rn soil emission rate of 0.73 atoms cm^{-2} s^{-1} based on a ^{222}Rn soil flux map for Europe from *Szegvary* [2007] and corresponding to the grid cell in which Bern is situated. The uncertainty in the ^{222}Rn soil flux is assumed to be about 25% [*Szegvary*, 2007].

3. Application to Ambient Observations in Bern

3.1. Measurement Location

The single pair of observations approach was applied to ambient observations of CO_2 and ^{222}Rn concentrations and $\delta(O_2/N_2)$ sampled at the roof of our laboratory (46°57′04″N, 7°26′20″E, 575 m above sea level) in the center of the city of Bern; see Figure 2. The sampling location is marked with an "A," and the "B" indicator refers to a nearby waste incineration facility. The local wind distribution for the period of 1 May 2004 to 1 November 2011 is given in Figure 3. Wind speeds < 1 m s^{-1} are dominant with approximately 49% occurrence followed by 1–2 m s^{-1} (about 33%) and 2−3 m s^{-1} (<10%). Dominant wind directions are WSW (about 34% of the time), N (23%), and SE (20%). Since our sampling location is in the center of the city and slightly elevated compared to most of the surroundings, our observations are to a good degree representative for CO_2 emissions from Bern.

Bern is a relatively small capital with about 124,500 inhabitants. Of the total area of about 51.6 km^2, 45% consists of built area, 20% agricultural area, and about 35% forests and parks [*Swiss Federal Statistical Office*, 2012]. Mean anthropogenic CO_2 emissions for Bern are estimated at 12.1 kt km^{-2} a^{-1} [*Stillhardt*, 2009]. About 28% of the fossil fuel-based CO_2 emissions are from natural gas combustion which is mostly used for heating purposes [*Klimagasbilanz für die Stadt Bern*, 2009].

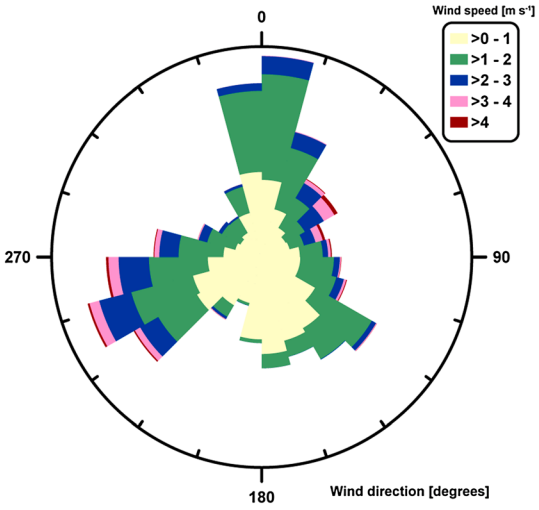

Figure 3. Distribution of local wind speeds and directions. Wind speeds 2 m s^{-1} and wind direction WSW are dominant with approximately 80% and 35% occurrence, respectively.

3.2. Measurement Equipment

The air is sampled from an aspirated intake on the roof of our laboratory (approximately 15 m above ground level) and transported down to the laboratory with a pump (KNF Neuberger, Switzerland, model N86KNDC with EPDM (ethylene propylene diene monomer) diaphragm) using Dekabon tubing (Synflex, 40 m long, 6 mm outer diameter) and cryogenically cooled to < -80°C to remove water vapor from the sample air. Concentrations of CO_2 and $\delta(O_2/N_2)$ are measured for each 10 min interval using an isotope ratio mass spectrometer (DELTAplusXP, Thermo Electron, Bremen, Germany).

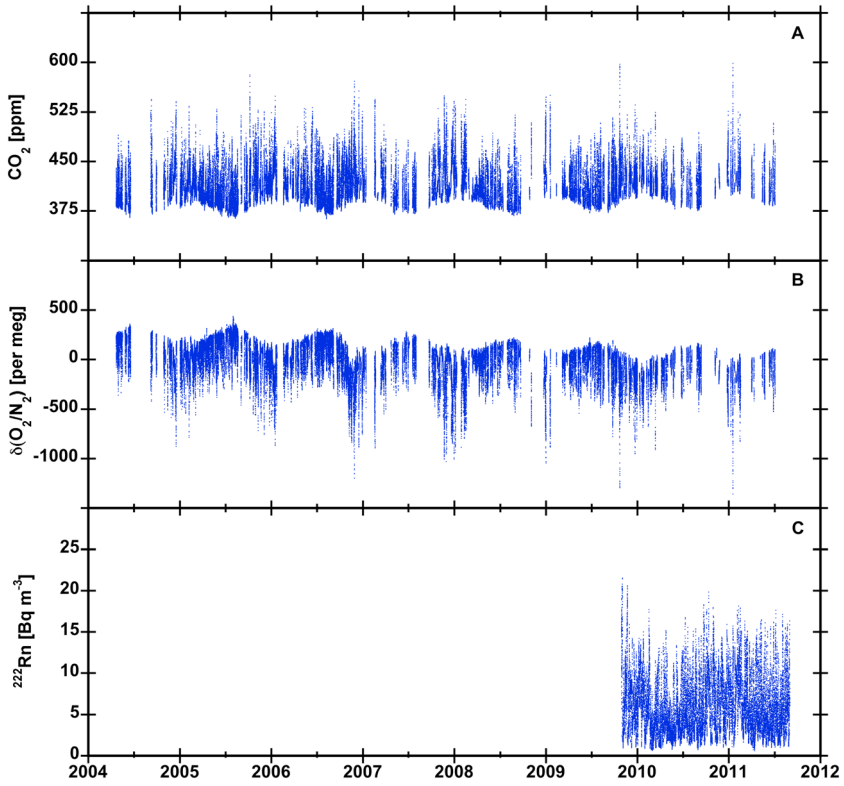

Figure 4. Ambient observations of (a) CO_2, (b) $\delta(O_2/N_2)$, and (c) ^{222}Rn.

CO_2 is measured as the ratio of CO_2 to N_2 and the obtained δ value is converted to a CO_2 concentration with a well-known reference gas with a concentration of 396.2 ppm. CO_2 is expressed in parts per million on the WMO2007X scale and $\delta(O_2/N_2)$ in per meg (1 ppm = 1/0.20946 = 4.8 per meg) on the Scripps scale. Measurement precision and accuracy are generally < 0.5 ppm for CO_2 and < 10 per meg for $\delta(O_2/N_2)$. For more details see *Leuenberger et al.* [2000] and *Sturm et al.* [2006]. ^{222}Rn activity is measured with a dual-flow loop/two-filter ANSTO Radon monitor [*Whittlestone and Zahorowski*, 1998] which is installed on the roof of our building. The measurement precision is dependent on the amount of counts and is about 6% at 1 Bq and 4% at 10 Bq. The accuracy depends mostly on the applied calibration standard and is estimated at about 6% for our observation period. Figure 4 shows the ambient observations of CO_2, $\delta(O_2/N_2)$ (from 1 May 2004 to 1 November 2011) and ^{222}Rn (1 November 2009 to 1 November 2011) as observed at the roof of our building. Data gaps are explained by flask measurements occupying the mass spectrometer [*Uglietti et al.*, 2008; *van der Laan-Luijkx et al.*, 2012] or technical problems.

3.3. Event Selection

Events are selected based on the CO_2 observations using the following definitions: The start is defined when at least five out of six consecutive points are higher than the one before and the first value (at t_1) has to be at least 1 ppm higher than the baseline (at t_0). The end of an event is defined as the maximum value before declination to the background level and is defined to have at least three out of five consecutive observations which are lower than the one before. For each event the CO_2 fluxes are calculated using equation (5) for each observation relative to the background level at the start of the event (i.e., at t_0). This way, we oversample nearby emissions but this makes sense considering the small of 2–3 km of Bern relative to our location. Similarly, the oxidative ratio (OR), i.e., the ratio of $\delta(O_2/N_2)$ to CO_2 is also calculated for each set of observations in the event with respect to the background. In total, 303 events were selected for $CO_2/^{222}Rn$ and 1423 events in the case for $\delta(O_2/N_2)$.

4. Results

4.1. CO_2 Surface Fluxes and OR

Figure 5a shows the results for our observed net CO_2 emissions and the OR is given in Figure 5b. In total, 5413 CO_2 fluxes and 24,203 ORs were calculated. The OR values are fitted with a single harmonic function to illustrate

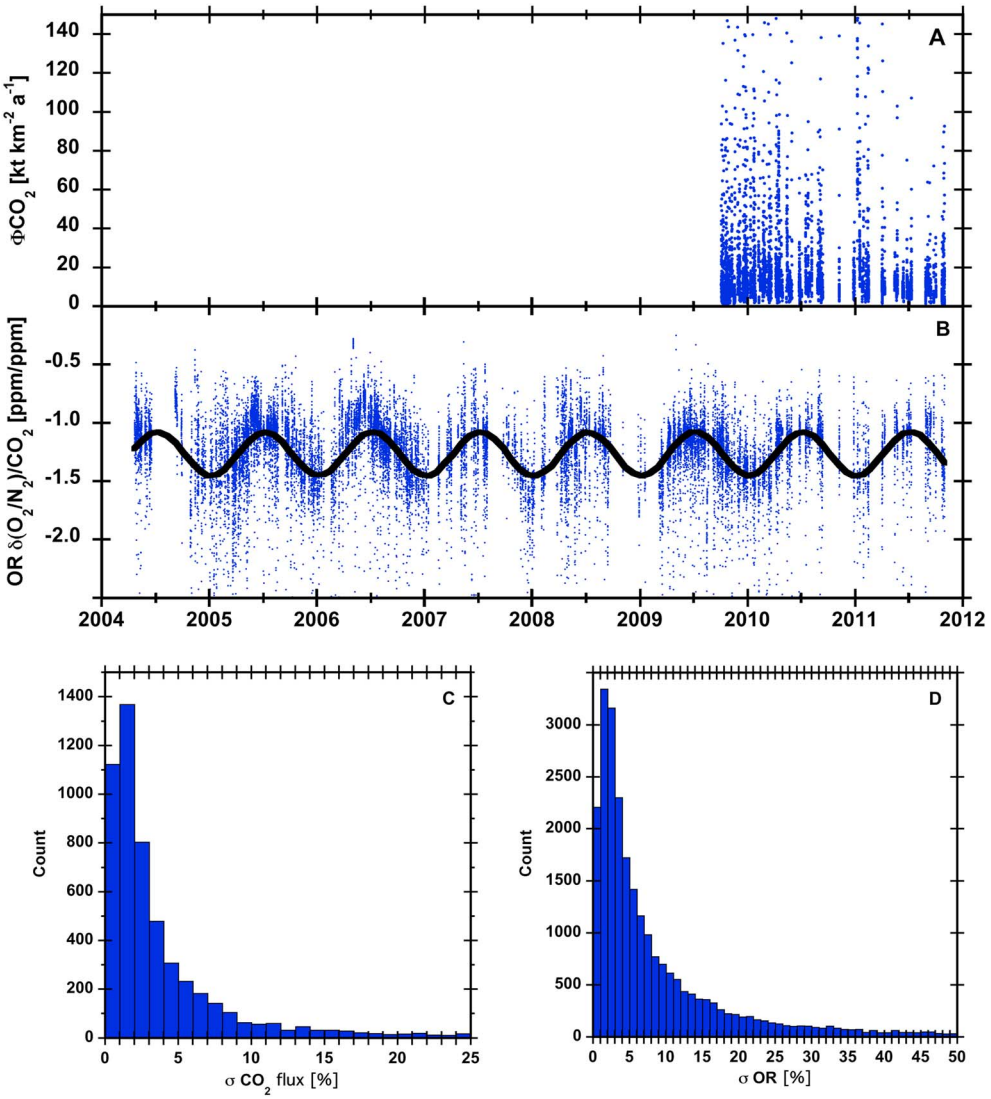

Figure 5. (a) Net CO_2 surface emissions and (b) oxidative ratios for the city of Bern. The latter is fitted with a single harmonic regression fit to indicate the seasonality with strong influence from the local biosphere in summer/spring and fossil fuel combustion processes in winter/autumn. The distribution of the random uncertainties for (c) Φ CO_2 and (d) OR are given, respectively.

the seasonality. More negative OR values are observed in winters due to fossil fuel combustion [*Keeling*, 1988], and less negative OR values of about −1 are observed in summers indicating strong influence from the local biosphere [*Severinghaus*, 1995].

The statistical distributions of their relative uncertainties (calculated by error propagation of equation (5) and the measurement precisions) are given in Figures 5c and 5d, respectively. For further analysis we applied a maximum uncertainty threshold of 25% for CO_2 fluxes and 20% for the OR observations. Furthermore, we only accepted OR values between 0 and −2.5 to remove outliers. This leaves 5262 values for the CO_2 fluxes of which 2880 are in winter/autumn and 2382 are in summer/spring. For the OR this leaves 21,574 values of which 7857 are in winter/autumn and 13,717 are in summer/spring.

4.2. Seasonal Variability and Annual Means

Figures 6a and 6b show the results for the CO_2 emissions for summer/spring and winter/autumn, respectively. For summer/spring, the median of the observations is 10.0 kt km^{-2} a^{-1} which is only slightly lower compared to the median in winter/autumn of 12.3 kt km^{-2} a^{-1}, but in winter/autumn higher values are observed much more often. Based on these results, we estimate net CO_2 emissions for the period of November 2009 to November

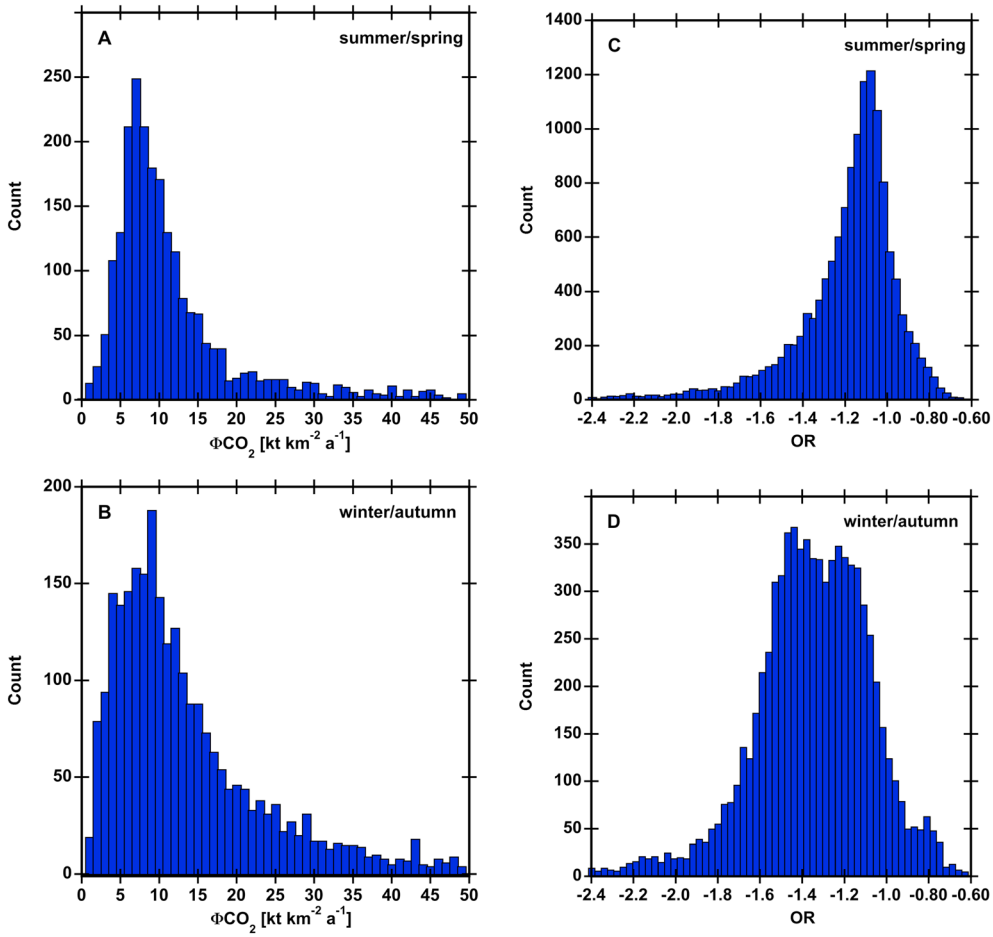

Figure 6. Net CO_2 surface emissions for (a) summer/spring and (b) winter/autumn and oxidative ratios for (c) summer/spring and (d) winter/autumn.

2011 at 11.2 ± 2.9 kt km^{-2} a^{-1} which is comparable to the reported emissions of 12.1 kt km^{-2} a^{-1} from fossil fuels alone. In summer/spring, the OR (Figure 6c) is centered around -1.1 indicating that our observations are influenced to a large degree by the local biosphere. However, much lower values are also observed indicating emission from fossil fuels. The very negative values (e.g., < -1.6) indicate significant contribution from natural gas combustion processes (i.e., having an OR of -2) which, in summer, are mainly attributed to cooking purposes and industry. Figure 6d shows a much broader population of the spectrum for the OR in winter/autumn with a cluster around -1.1 and a second cluster around -1.5 indicating a significant influence from the local biosphere (i.e., mostly biospheric respiration) and anthropogenic emission sources. A significant part of the OR observations (i.e., OR < -1.6) is to a large degree attributed to local natural gas combustion processes which is mainly used for heating purposes. Our results are summarized in Table 2 and include the random uncertainties as calculated by the propagation of the respective measurement errors (section 3.2) in equation (5). Annual mean estimates (discussed later) include also the systematic uncertainty which, in the case for the CO_2 fluxes, mainly represents the accuracy of the ^{222}Rn measurements and uncertainty due to the assumed ^{222}Rn soil flux.

Table 2. Results for Net CO_2 Emission and OR[a]

	Summer/Spring	Winter/Autumn	Annual Mean	
Φ_{CO2}	10.0 ± 0.5	12.3 ± 0.6	11.2 ± 2.9	kt km^{-2} a^{-1}
OR	-1.1 ± 0.1	-1.3 ± 0.1	-1.2 ± 0.1	kt km^{-2} a^{-1}

[a]Seasonal results are given with random errors based on the measurement precisions and error propagation of equation (5). Annual mean includes also the systematic uncertainty.

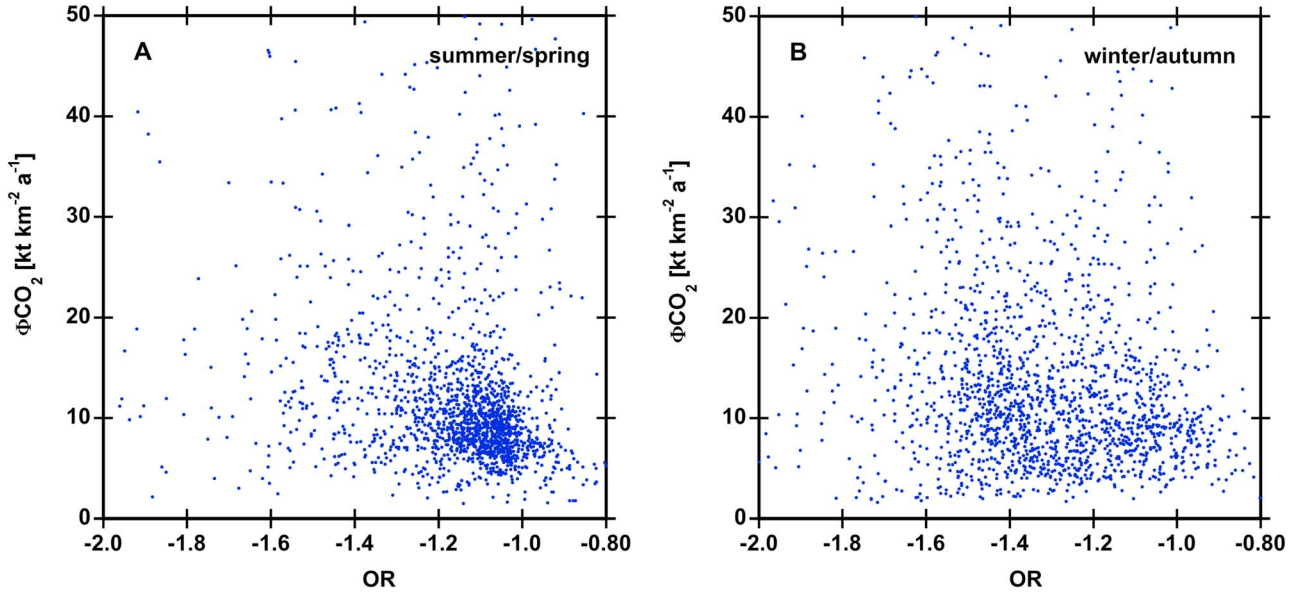

Figure 7. Net CO_2 surface emissions versus oxidative ratios for (a) summer/spring and (b) winter/autumn.

Figures 7a (summer/spring) and 7b (winter/autumn) show the CO_2 flux versus the OR. The OR values close to -1 represent local biosphere emissions and a negligible amount of mixing with other sources. The values suggest that the net emissions from the local biosphere are roughly < 10 kt km^{-2} a^{-1}. Our observations indicate a large variability in both net CO_2 emissions and OR but there is a slight tendency for higher net CO_2 emissions at more negative ORs. In summer/spring, this can be explained by uptake of CO_2 by the local biosphere. In winter/autumn however, most of the influence from the biosphere is related to respiration (i.e., less photosynthesis). Therefore, the data suggest that the highest CO_2 emissions are dominantly from fossil fuel combustion processes.

4.3. Spatial Distribution

The spatial distribution of our observed CO_2 sources is shown in Figures 8a–8d where the observed CO_2 flux and OR are plotted against the wind direction and the maximum distance of influence (MDI). The latter is calculated from the (transit) time between the observations at t_0 and t_n and the local wind speed. For example, the MDI corresponding to a net flux calculated from (10 min integrated) observations sampled at t_5 relative to local background conditions (i.e., sampled at t_0) and a local wind speed of 1 m s^{-1} at t_0 and 2 m s^{-1} at t_5 would be $1.5\,\mathrm{m\,s^{-1}} \cdot 5 \cdot 600\,\mathrm{s} = 4.5$ km. We use the term MDI instead of distance because the distances are potentially overestimated because of mixing with nearby sources and sinks. For example, clean air from the outer sectors will seem polluted after mixing with nearby emission sources. Spatial attribution is therefore mostly accurate for nearby sources.

Both in summer/spring (Figure 8a) and winter/autumn (Figure 8b), a large variability in net CO_2 emissions is observed which is relatively evenly spread throughout our footprint. However, the results for the OR indicate a significant change from a dominant biospheric source in summer/spring (Figure 8c) to anthropogenic sources in winter/autumn (Figure 8d). In summer/spring, most of our observed footprint is strongly influenced by biospheric activity. Several point sources are however observed with very negative OR values (i.e., < -1.5) suggesting significant contributions from natural gas combustion, which in summer/spring originate mainly from households (e.g., cooking and showering) and industry.

At about 2 km west of our sampling location (Figure 2) a large waste incineration facility is located. The facility is, on a yearly basis, responsible for approximately 10% of the total anthropogenic CO_2 emissions in Bern and accounts for 35% of the CO_2 emissions from natural gas consumption [*Klimagasbilanz für die Stadt Bern*, 2009]. The facility seems to appear in Figure 8c (for which we have the most data) at around 250° and also at 300°. Since we only know of one large point source west to our site, we attribute the double appearance to local meteorological conditions and orography. In winter/autumn (Figure 8d) the facility is less obvious because much more fossil fuels are combusted throughout the city in this period, especially natural gas which is used for heating purposes.

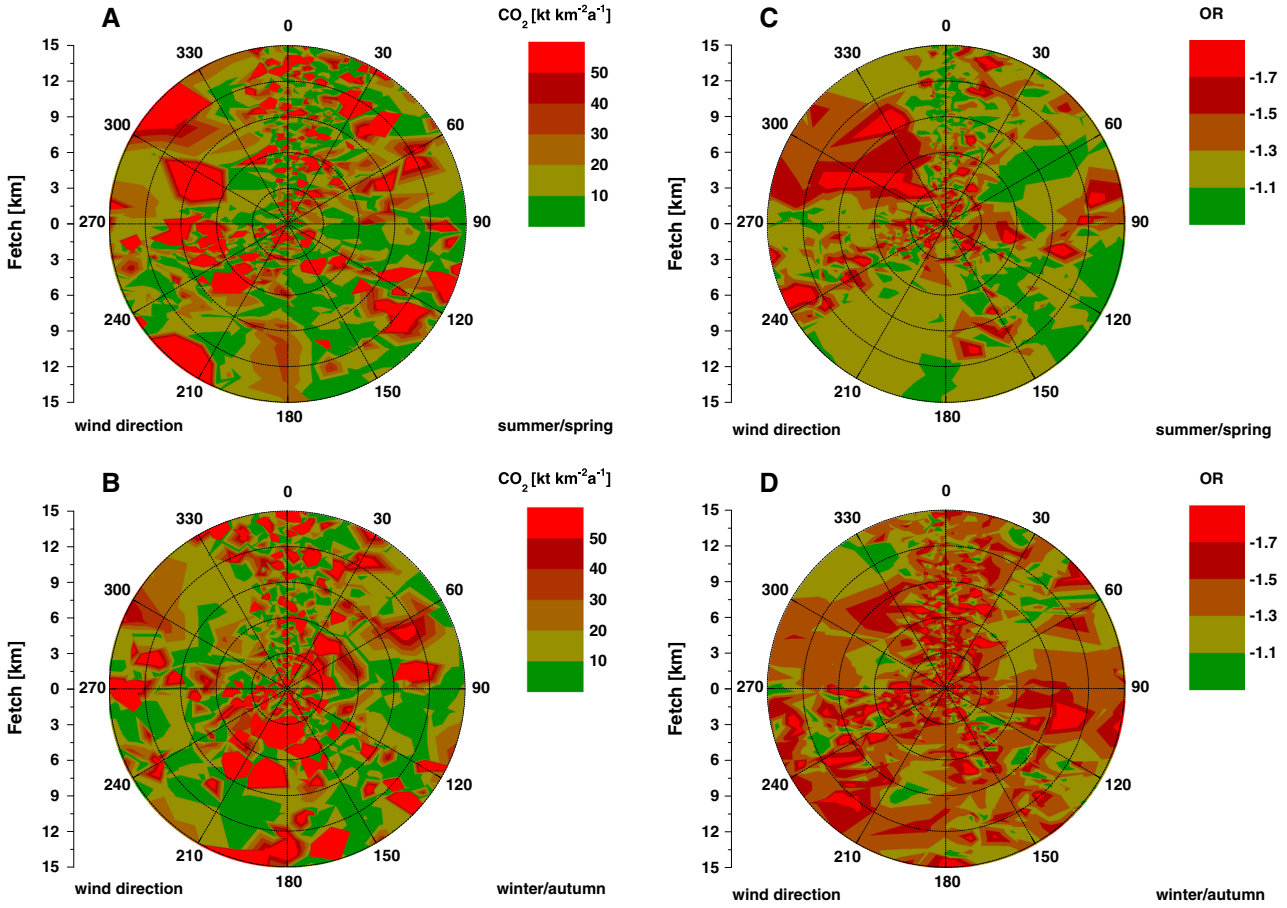

Figure 8. Spatial distribution of net CO_2 surface emissions for (a) summer/spring and (b) winter/autumn and oxidative ratios for (c) summer/spring and (d) winter/autumn. The maximum distance of influence (MDI) is estimated from the transit time of the air mass and local wind speed.

4.4. Diurnal Variability

Our single pair of observations approach allows for analysis at very high temporal resolutions. This is demonstrated in Figures 9a and 9b where the hourly medians and standard errors for all observed CO_2 emissions and OR values are shown. Figures 9a and 9b (green circles) represent the results for summer/spring and the red squares indicate the winter/autumn values. The *x* axis represents the corresponding mean observation time expressed as the hour of day. For example, for a CO_2 flux which is calculated from an observation at 17:00 and uses a background level observed at 15:00, the result is included in the median value at 16 h.

Because our methodology requires relatively stable atmospheric conditions, observations around midday are highly underrepresented especially for the CO_2 fluxes. Still, a clear distinction between the day and night is visible in both figures. OR values are lowest between about 7 h and 18 h when observed CO_2 emissions are dominantly from fossil fuel combustion processes. During the winter/autumn observed ORs are generally -1.6 around midday with a lowest mean value of -1.77. This can only be explained by a dominant fraction of CO_2 emissions from natural gas combustion processes (i.e., from heating and cooking) since such a process would yield an OR of -2.

Nighttime (i.e., between 19 h and 7 h) CO_2 emissions were estimated at 13.5 kt km^{-2} a^{-1} for summer/spring and 13.7 kt km^{-2} a^{-1} for winter/autumn (both median values). These values are surprisingly similar since the OR observations show a significant shift from -1.25 in summer/spring to -1.40 in winter/autumn. This suggests that, compared to summer/spring, the larger contribution from local fossil fuel sources in winter/autumn is compensated by the smaller fraction of biospheric respiration (due to lower soil temperatures).

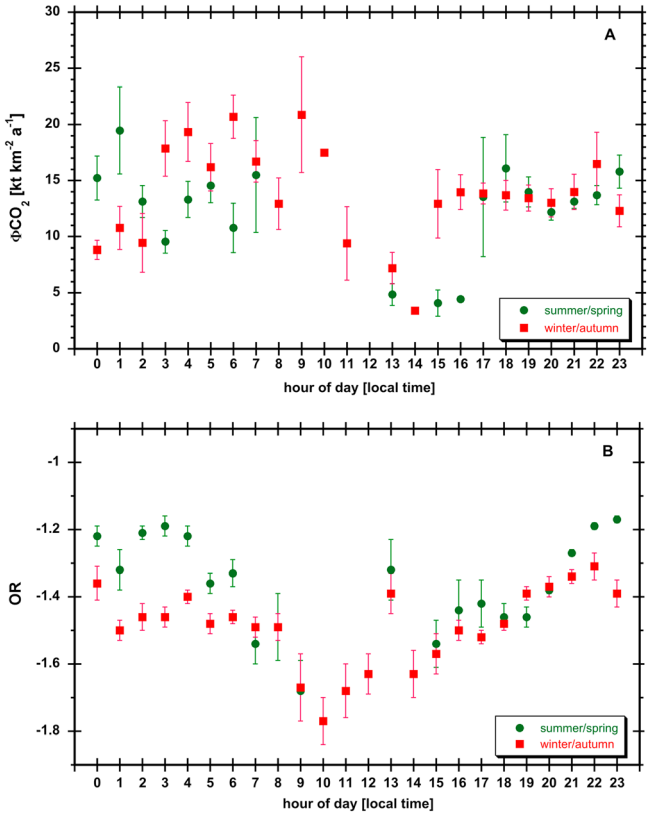

Figure 9. Hourly variability of (a) net CO_2 surface emissions and (b) oxidative ratios. Summer/spring values are indicated with the green circles and winter/autumn with the red squares.

5. Discussion and Conclusions

We have demonstrated a modified approach to the ^{222}Rn inversion method based on single pairs of ^{222}Rn and CO_2 observations during stable atmospheric conditions. The method is a useful alternative to the commonly applied technique of using a linear regression fit on a bulk of observations because it accounts for nonstationary CO_2 sources. The single-pair approach therefore offers the potential to better constrain local to regional net surface emissions and the theory applies, in principle, equally to other observed concentration ratios (e.g., $\delta^{13}C/CO_2$).

Similar to the standard approach our method is equally limited to the assumption of a constant (and well-known) ^{222}Rn surface flux and a stable planetary boundary layer (PBL) height during the observation period. The PBL height determines the height of the observed concentrations. Therefore, if for a certain part of the trajectory the PBL height is (suddenly) lower, then those emissions will be overestimated. This implies that in cases when the PBL gradually decreases, the results will be biased toward nearby emissions. The ^{222}Rn soil emission rate is important because the results for the CO_2 emissions are directly proportional to the assumed value. For this work, the uncertainty related to the ^{222}Rn surface flux is estimated at about 25% [*Szegvary*, 2007]. However, since this uncertainty is systematic, long-term trends can be assessed with much greater confidence. On hourly time scales the variability of the ^{222}Rn surface flux can potentially be much larger because even though the production rate of ^{222}Rn is constant, its soil emanation depends also on atmospheric pressure and soil texture, temperature, and humidity. Furthermore, it is clear that for some of the higher chimneys the dispersion for CO_2 differs from that of (the ground-based) ^{222}Rn. For these reasons, and because of statistics, we have based our emission estimates on 2 years of data and calculated the fluxes and ORs using all observations within each event, relative to local background values. Since the above named uncertainties are expected to increase with longer events, it is recommended to utilize an atmospheric transport model [e.g., *van der Laan et al.*, 2010] as an independent mean to validate the results when using our approach to nonlocal emission estimates.

Based on the results for summer/spring and winter/autumn the annual mean net CO_2 emissions for Bern are estimated at 11.2 ± 2.9 kt km^{-2} a^{-1} for the period of November 2009 to November 2011. This value is, within

the uncertainty estimates, comparable to the reported CO_2 emissions of 12.1 kt km^{-2} a^{-1} from fossil fuels alone. Assuming our applied ^{222}Rn soil flux is accurate, this would suggest that the local biosphere acts neither as a net source nor as a net sink for CO_2 on a yearly basis. However, because our methodology requires relatively stable atmospheric conditions, our results are biased toward nocturnal CO_2 emissions. This means that our results are biased toward biospheric respiration and nocturnal fossil fuel sources and underestimate daytime emission sources (e.g., traffic) and uptake from photosynthesis. In a future study we hope therefore to partition between the local biosphere and fossil fuel sources using $^{14}CO_2$ observations.

Our OR observations have provided valuable information about the spatial and temporal variability of the local emission sources. Except for a large nearby waste incineration facility, most emission sources are relatively evenly spread throughout our catchment area. During the period of 1 May 2004 to 1 November 2011, a mean OR was observed of -1.2 ± 0.1. For the nighttime observations, a significant shift from biospheric respiration to fossil fuel combustion processes was observed from summer/spring to winter/autumn with a mean OR decreasing from -1.25 to -1.40, respectively. Our data are in line with the expected pattern of increased gas usage in winter/autumn and dominantly during the daytime. Considering all of the above, the approach presented in this paper provides a valuable tool to monitor long-term trends in CO_2 emissions for the city of Bern.

Acknowledgments

This work was partly supported by the Swiss National Science Foundation and the Federal Office for Meteorology and Climatology MeteoSwiss in the framework of Swiss GCOS activities. We are grateful to Wlodek Zahorowski for providing the radon detector operated in Bern. The authors thank Peter Nyfeler for setting up the measurements and his extensive work in our laboratory and Gerko van der Wel for his contributions to the data processing. We furthermore would like to thank our three anonymous reviewers whose comments have greatly helped us to improve the final version of this manuscript.

References

Biraud, S., P. Ciais, M. Ramonet, P. Simmonds, V. Kazan, P. Monfray, S. O'Doherty, T. G. Spain, and S. G. Jennings (2000), European greenhouse gas emissions estimated from continuous atmospheric measurements and radon-222 at Mace Head, Ireland, *J. Geophys. Res.*, *105*(D1), 1351–1366.

Hirsch, A. I. (2007), On using radon-222 and CO_2 to calculate regional-scale CO_2 fluxes, *Atmos. Chem. Phys.*, *7*(14), 3737–3747, doi:10.5194/acp-7-3737-2007.

Keeling, R. F. (1988), Measuring correlations between atmospheric oxygen and carbon-dioxide mole fractions—A preliminary study in urban air, *J. Atmos. Chem.*, *7*, 153–176, doi:10.1007/BF00048044.

Klimagasbilanz für die Stadt Bern (2009), Rückschluss auf das Jahr 2008, Amt fur umweltschutz und lebensmittelkontrolle der stadt Bern. [Available at http://www.bern.ch/leben_in_bern/sicherheit/umweltschutz/energie/bernlebenslage.2006-09-21.8260622339/klimagasbilanz_2008.pdf.]

Leuenberger, M., P. Nyfeler, H. P. Moret, P. Sturm, A. Indermühle, and J. Schwander (2000), CO_2 concentration measurements on air samples by mass spectrometry, *Rapid Commun. Mass Spectrom.*, *14*(16), 1552–1557.

Levin, I. (1987), Atmospheric CO_2 in continental Europe—An alternative approach to clean air CO_2 data, *Tellus B*, *39B*(1-2), 21–28, doi:10.1111/j.1600-0889.1987.tb00267.x.

Messager, C., M. Schmidt, M. Ramonet, P. Bousquet, P. Simmonds, A. Manning, V. Kazan, G. Spain, S. G. Jennings, and P. Ciais (2008), Ten years of CO_2, CH_4, CO and N_2O fluxes over Western Europe inferred from atmospheric measurements at Mace Head, Ireland, *Atmos. Chem. Phys. Discuss.*, *8*(1), 1191–1237, doi:10.5194/acpd-8-1191-2008.

Popa, M. E., A. T. Vermeulen, W. C. M. van den Bulk, P. A. C. Jongejan, A. M. Batenburg, W. Zahorowski, and T. Röckmann (2011), H_2 vertical profiles in the continental boundary layer: Measurements at the Cabauw tall tower in the Netherlands, *Atmos. Chem. Phys.*, *11*(2), 6425–6443, doi:10.5194/acp-11-6425-2011.

Schmidt, M., R. Graul, H. Sartorius, and I. Levin (1996), Carbon dioxide and methane in continental Europe: A climatology, and ^{222}Radon-based emission estimates, *Tellus B*, *48*(4), 457–473.

Schmidt, M., H. Glatzel-Mattheier, H. Sartorius, D. E. Worthy, and I. Levin (2001), Western European N_2O emissions: A top-down approach based on atmospheric observations, *J. Geophys. Res.*, *106*(D6), 5507–5516.

Severinghaus, J. P. (1995), Studies of the terrestrial O_2 and carbon cycles in sand dune gases and in biosphere 2, PhD thesis, Columbia Univ., New York, 148 pp.

Stillhardt, B. (2009), Klimagasbilanz für die Stadt Bern, Aktualisierung auf das Jahr 2008 *Rep*., amt für umweltschutz der stadt Bern, Umwelt & Energie, Energiefachstelle, Brunngasse 30, 3000 Bern, Bern.

Sturm, P., M. Leuenberger, F. L. Valentino, B. Lehmann, and B. Ihly (2006), Measurements of CO_2, its stable isotopes, O_2/N_2, and ^{222}Rn at Bern, Switzerland, *Atmos. Chem. Phys.*, *6*(7), 1991–2004, doi:10.5194/acp-6-1991-2006.

Swiss Federal Statistical Office (2012), City of Bern, key data. [Available at http://www.bfs.admin.ch/bfs/portal/en/index/regionen/regionalportraets/bern/blank/key.html.]

Szegvary, T. (2007), European ^{222}Rn flux map for atmospheric tracer applications, PhD thesis, Institute of Environmental Geosciences, University of Basel, Switzerland, Basel.

Uglietti, C., M. Leuenberger, and F. L. Valentino (2008), Comparison between real time and flask measurements of atmospheric O_2 and CO_2 performed at the High Altitude Research Station Jungfraujoch, Switzerland, *Sci. Total Environ.*, *391*(2-3), 196–202.

van der Laan, S., R. E. M. Neubert, and H. A. J. Meijer (2009), Methane and nitrous oxide emissions in the Netherlands: Ambient measurements support the national inventories, *Atmos. Chem. Phys.*, *9*(24), 9369–9379, doi:10.5194/acp-9-9369-2009.

van der Laan, S., U. Karstens, R. E. M. Neubert, I. T. van der Laan-Luijkx, and H. A. J. Meijer (2010), Observation-based estimates of fossil fuel-derived CO_2 emissions in the Netherlands using $\Delta^{14}C$, CO and ^{222}Radon, *Tellus B*, *62*(5), 389–402, doi:10.1111/j.1600-0889.2010.00493.x.

van der Laan-Luijkx, I. T., et al. (2012), Atmospheric CO_2, $\delta(O_2/N_2)$ and $\delta^{13}CO_2$ measurements at Jungfraujoch, Switzerland: Results from a flask sampling intercomparison program, *Atmos. Meas. Tech. Discuss.*, *5*(5), 7293–7322, doi:10.5194/amtd-5-7293-2012.

Whittlestone, S., and W. Zahorowski (1998), Baseline radon detectors for shipboard use: Development and deployment in the First Aerosol Characterization Experiment (ACE 1), *J. Geophys. Res.*, *103*(D13), 16,743–16,751, doi:10.1029/98JD00687.

Wilson, S. R., A. L. Dick, P. J. Fraser, and S. Whittlestone (1997), Nitrous oxide flux estimates for south-eastern Australia, *J. Atmos. Chem.*, *26*(2), 169–188.

Yver, C., M. Schmidt, P. Bousquet, and M. Ramonet (2010), Measurements of molecular hydrogen and carbon monoxide on the Trainou tall tower, *Tellus B*, *63*(1), 52–63, doi:10.1111/j.1600-0889.2010.00520.x.